coatings

Article

Research on the Influence of Process Parameters on the Flow Field in Mold

Fengming Du [1], Jian Zhao [2], Yue Zheng [3], Tianyi Li [4] and Gengtao Zheng [5,*]

1 International Shipping Research Institute, GongQing Institute of Science and Technology, Jiujiang 332020, China
2 IFE Elevators Co., Ltd., Dongguan 523648, China
3 Faraday Future Company, Shanghai 201106, China
4 Offshore Oil Engineering Co., Ltd., Tianjin 300461, China
5 College of Marine Engineering, Dalian Maritime University, Dalian 116000, China
* Correspondence: guanghuisuiyue0504@163.com

Abstract: The mold is one of the core components of steelmaking, and its flow field distribution will directly affect the quality of the casting slab. A three-dimensional nozzle model is built in this work, and fluid simulation is carried out to investigate the influence of the casting speed, immersion depth, slab thickness, and width on flow behavior in the mold. This model combined simulation with real conditions. The casting speed, immersion depth, slab width, and slab thickness are the actual process parameters used in the steel factory. The results show that when the casting speed increases from 0.6 to 1.0 m/min, the strike positions of the narrow surface are 0.439, 0.476, and 0.480 m below the liquid level, respectively. When the immersion depth increases from 180 to 220 mm, the impact depth of the stream at the exit of the nozzle side hole moves down, the lower recirculation zone moves to the centre and bottom of the slab, and the upper recirculation zone moves downward. When the slab thickness increases, the strike locations of the narrow face move down. Further, when the slab width increases, the distance of the strike location from the strike position increases first and then decreases. From the fluid results, the process parameters can be optimized by considering the strike location and the change of the surface turbulent kinetic energy. The model proposed in this work provides a theoretical guidance and optimization for the nozzle.

Keywords: continuous casting; nozzle; mold; flow; impact

check for updates

Citation: Du, F.; Zhao, J.; Zheng, Y.; Li, T.; Zheng, G. Research on the Influence of Process Parameters on the Flow Field in Mold. *Coatings* **2022**, *12*, 1547. https://doi.org/10.3390/coatings12101547

Academic Editor: Rafael Taboryski

Received: 7 September 2022
Accepted: 10 October 2022
Published: 14 October 2022

1. Introduction

Continuous casting production is a crucial component of the steel industry. The process involves high-temperature liquid molten steel being injected into a mold from the tundish through a submerged entry nozzle (SEN), where the initial solidified shell is formed under the cooling effect of the mold's copper plate. The mold is known as the heart of the continuous casting machine and is the key factor determining the quality of the slab [1–6]. The flow of molten steel in the mold has become the focus of research attention in recent years. Analysis of the complex process in the mold has been facilitated by improvements in computing power and the rapid development of numerical simulation methods. The flow of molten steel affects the solidification of the casting slab and the uniformity of the solidified billet shell, and directly determines the occurrence of defects, such as cracks. In actual production, the change of process parameters will have a direct impact on the flow of molten steel; thus, it is meaningful to research the influence of process parameters, such as pulling speed, immersion depth, slab thickness, and width, on flow behavior in the mold [7–10].

Many scholars have previously analyzed the flow characteristics in a mold. For example, Ho et al. [11] studied the effect of flow pattern on the fluid field and inclusions in the mold. According to their findings, an increase in the pulling speed reduced the residence time, which had an adverse effect on the removal of inclusions. The results were meaningful for the optimization of SEN design. Yang et al. [12] developed a 3D model to describe molten steel flow, the solidification process, and heat transfer in the mold. They observed the formation mechanism of macrosegregation, calculated the thickness and the temperature of the slab at the liquid phase cavity, and, then, verified the findings with the measured values. The results showed that the temperature in the middle of the fluid steel was lower than the temperature of the fluid steel at the solidification front due to circulation in the reflow zone. This made the solidified billet grow unevenly and caused quality defects, such as shrinkage and segregation of the billet. Thomas and Zhang [13] studied the mathematical model of the mold flow field in slab continuous casting, employing one-phase and two-phase model research, water model experiments, particle image velocimetry digital imaging, and volume of fluid model surface topography simulation. Wang et al. [14] built a three-dimensional transient model which allowed for the complex phenomenon in the mold. They researched the parameters, such as temperature, speed, surface profile, fluid pattern, and so on. The model could enable a deep understanding of the fluid field. Tian et al. [15] proposed a new method to conveniently measure the speed distribution in the mold. They considered the temperature, thermoelectric force, and speed through the Seebeck effect. The online detection was also used to verify the speed distribution. Domitner et al. [16] calculated the influence of the casting speed on the slab quality; they believed that the speed influenced the metallurgical length of the slab.

Although many researchers have studied the flow of molten steel in the mold, there are still few reports which consider the casting speed, immersion depth, slab thickness, and width on flow behavior [17–19]. The condition parameters are important factors that affect the slab quality; therefore, this work builds a 3D nozzle model in which the casting speed, immersion depth, slab thickness, and width can be changed. All the parameters in this study are the real-condition parameters from the steel factory.

2. Fluid Model

Figure 1 provides a structural diagram of the SEN. The structure is a double-sided mouth; the inner diameter is 98 mm, and the size of the oval is 54 mm × 90 mm.

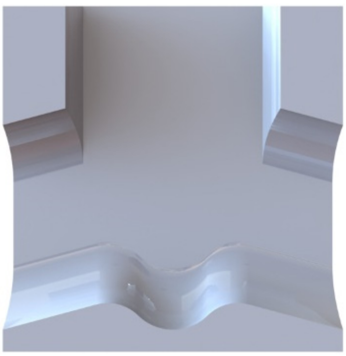

Figure 1. The structures of SEN.

The detailed parameters of the model are shown in Table 1. The mesh of the model is shown in Figure 2. The time step is 0.01 s and the iterations number is 5000. The grid is hexahedral mesh and the number is 456,951.

Table 1. Calculation parameters.

Item	Value
Length of mold	900 mm
Liquid level height	100 mm
Immersion depth of nozzle	130 mm
Casting speed	$0.8\ \mathrm{m \cdot min^{-1}}$
Steel density	$7200\ \mathrm{kg \cdot m^{-3}}$
Steel viscosity	$0.0055\ \mathrm{kg \cdot m^{-1} \cdot s^{-1}}$

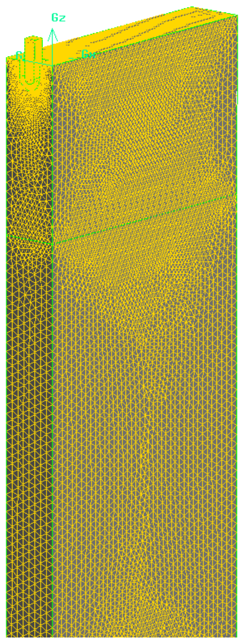

Figure 2. The mesh of the model. x, y, z are the directions.

Here are the assumptions.

(1) Molten steel is regarded as being in an incompressible steady state;
(2) Ignore the vibration of the mold and slag flow;
(3) The natural convection caused by density changes is ignored. The rapid outflow of molten steel from the nozzle impinges on the molten steel in the mold, causing forced convection; however, the density change of molten steel is very small, and the natural convection caused by the density change is far smaller than the forced convection caused by the impact of molten steel, so it can be ignored;
(4) The calculation boundary is a no-slip boundary. In general, large-scale flow field analysis, the wall belongs to a no-slip boundary. For microchannels, slip boundary conditions can be considered to make the numerical results consistent with the actual situation. In this paper, the simulation belongs to large-scale analysis, we focus on the macroscopic flow field results, and there is no need to use a slip boundary. Almost all the references concerning flow calculation of steel in the mold adopt no-slip boundary conditions.

Here are the governing equations:

(1) Continuity equation:

$$\rho \frac{\partial (v_i)}{\partial x_i} = 0 \tag{1}$$

where v_i denotes the velocity vector, ρ is the density, and x_i denotes the coordinate.

(2) Momentum equation:

$$\rho\frac{\partial(v)}{\partial t}+\nabla\times(\rho vv)=-\nabla p+\nabla\times(\tau)+F \tag{2}$$

$$\tau=\mu\left[\left(\nabla v+\nabla v^{\mathrm{T}}\right)\right]-\frac{2}{3}\nabla\times vI \tag{3}$$

Here, p represents the pressure, F denotes the external volume force, τ denotes the stress tensor, and I represents the unit tensor.

(3) Energy-conservation equation:

$$\rho\frac{\partial(T)}{\partial \mathrm{t}}+\rho div(vT)=div\left(\frac{k}{c_\rho}gradT\right)+S_T \tag{4}$$

Here, c_ρ, T, K, and S_T denote the specific heat capacity, temperature, conductivity, and viscous dissipation term, respectively.

(4) Standard k-ε equation:

$$\rho\frac{\partial(v_j k)}{\partial x_j}=\frac{\partial}{\partial x_j}\left(\frac{\mu_\tau}{\sigma_k}\frac{\partial k}{\partial x_j}\right)+G_k-\rho\varepsilon \tag{5}$$

$$\rho\frac{\partial(v_j\varepsilon)}{\partial x_j}=\frac{\partial}{\partial x_j}\left(\frac{\mu_\tau}{\sigma_k}\frac{\partial\varepsilon}{\partial x_j}\right)+C_1G_k\frac{s}{k}-C_2\rho\frac{s^2}{k} \tag{6}$$

Here are the boundary conditions.

(1) The entry condition is the velocity entry;
(2) The exit condition is the velocity exit;
(3) The fluid level is free, and no shear force exists;
(4) Both the mold wall and nozzle wall are treated as non-slip solid walls, while the flow field near the wall is treated as a standard wall function.

3. Results and Discussion

3.1. Fluid Distribution under Different Casting Speeds

Figure 3 shows the flow field at three different casting speeds of 0.6, 0.8, and 1.0 m/min. The increase in casting speed makes the molten steel flow speed in the mold significantly faster, the momentum of the liquid molten steel increase, and the velocity distribution of the reflux areas change significantly. Table 2 lists the whirlpool centre locations and the strike locations of the narrow surface in the upper and lower recirculation zones of the flow field. The results show that when the casting speed is 0.6, 0.8, and 1.0 m/min, incrementally, the position of the whirlpool centre in the upper recirculation zone moves toward the nozzle and is relatively close to the liquid surface, while the position of the whirlpool centre in the lower reflux zone expands with the increase of the casting speed. The tendency and order of magnitude of the results are in agreement with the results simulated by Takatani et al. and Li et al. [20,21], they also agree with the experimental results proposed by Shamsi et al. and Lu et al. [22,23].

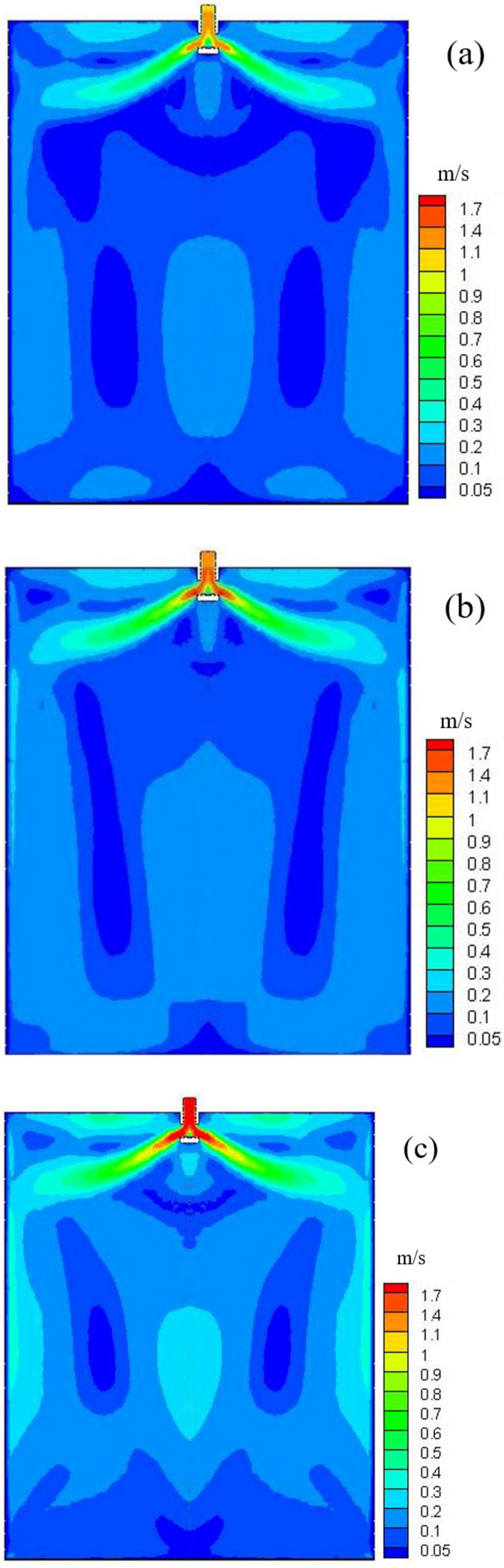

Figure 3. Flow contours of molten steel with different velocities: (**a**) 0.6 m/min; (**b**) 0.8 m/min; and (**c**) 1.0 m/min.

Table 2. Whirlpool core positions and strike locations under different casting speeds.

Speed	Upper Whirlpool Centre	Lower Whirlpool Centre	Strike Position
0.6 m·min^{-1}	(0.650 m, −0.247 m)	(0.596 m, −1.958 m)	−0.439 m
0.8 m·min^{-1}	(0.590 m, −0.247 m)	(0.613 m, −1.860 m)	−0.476 m
1.0 m·min^{-1}	(0.596 m, −0.237 m)	(0.605 m, −1.630 m)	−0.480 m

Figure 4 shows the flow velocity distribution of the free surface of the slab section at different casting speeds. When the casting speed increases, the free surface velocity becomes significantly faster. The distribution of the molten steel flow field is very sensitive to changes in the casting speed. The liquid level stability of the mold flow field will be affected when the speed is too low or too fast, which will influence the distribution of protective slag in the liquid level and result in a reduction in the quality of the casting billet.

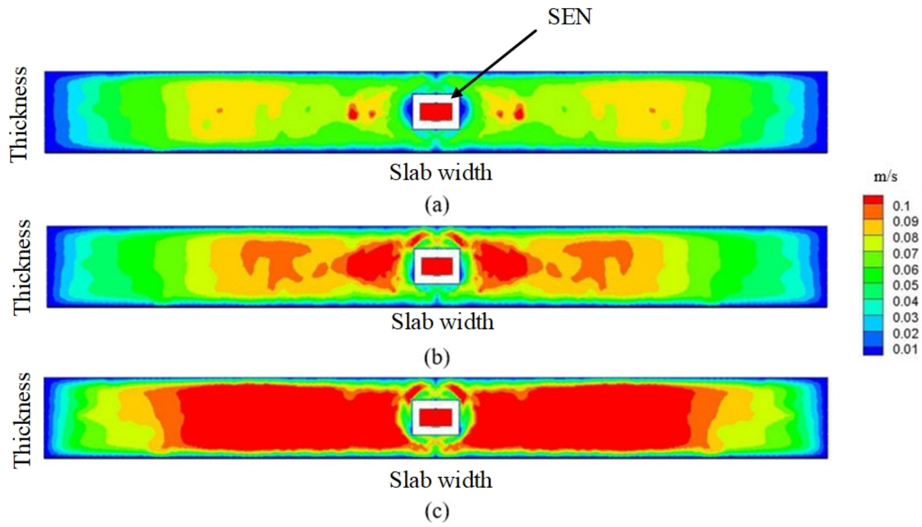

Figure 4. Velocity distribution of the free surface of the slab section under different velocities. (**a**) 0.6 m/min; (**b**) 0.8 m/min; and (**c**) 1.0 m/min.

Figure 5 provides a comparison of the turbulent kinetic energy on the free liquid surface at different casting speeds. When the speed is 0.6 m/min, the turbulent kinetic energy is low, and the maximum value is only 0.00078 m^2·s^{-2}, which shows a parabolic uniform change where the fluctuation of the liquid surface is small. When the speed is 0.8 m/min, the turbulent kinetic energy on the free liquid surface fluctuates up and down with a maximum value of 0.000978 m^2·s^{-2}, which appears 0.5 m away from the centre of the nozzle. When the speed is 1.0 m/min, compared with the previous two drawing speeds, the turbulent kinetic energy changes dramatically, with the maximum value reaching 0.00194 m^2·s^{-2}, which is approximately 2.5 times the maximum value at 0.6 m/min. Under these conditions, the free liquid surface will fluctuate violently, the melting stability of the slag will be destroyed, and bubbles and inclusions can easily occur. As the quality of the slab decreases markedly, it is necessary to be very careful when increasing the casting speed in actual production, and to prepare a reasonable nozzle plan.

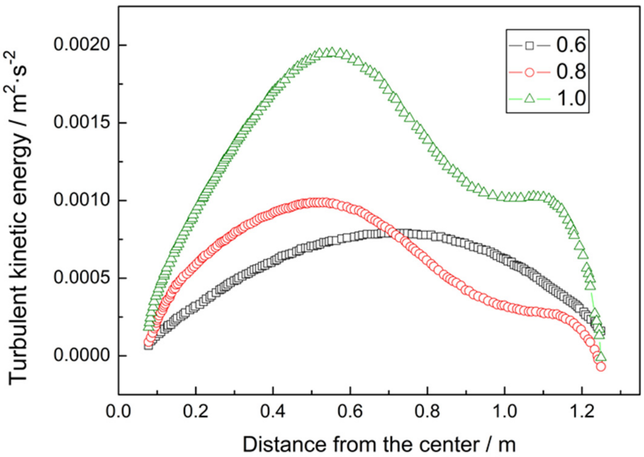

Figure 5. Turbulent kinetic energy at the free surface under different casting speeds.

3.2. Fluid Distribution under Different Immersion Depths

Figure 6 shows the flow lines of the molten steel in molds with nozzle immersion depths of 180, 200, and 220 mm. The location of the whirlpool centres and the strike locations of the narrow surface are shown in Table 3. It can be seen that when the immersion depth of the nozzle increases, the impact depth of the stream at the exit of the nozzle side hole moves down, the lower recirculation zone moves to the centre and bottom of the slab, and the upper recirculation zone moves downward. Meanwhile, the flow distance of the molten steel increases, the momentum is consumed, and the speed decreases when it reaches the free surface. When the immersion depth is small, the mold flux layer is relatively active, which is more conducive to the slag melting; however, it is easy to entrain the slag and inclusions under these conditions, and this affects the quality of the slab. If the immersion depth is large, the activity of the molten steel surface decreases, which is not conducive to mold flux. The heat transfer between the slag, the slab shell, and the mold's copper plate is hindered, and crack bonding is prone to occur. The solidification bridge of the mold slag between the nozzle and the mold's copper plate is not conducive to the normal solidification of the slab, and the temperature of the molten steel is higher at this point. Therefore, the selection of immersion depth generally follows the principle of controlling the fluctuation of the free liquid surface within a reasonable range, where the smaller the immersion depth, the better.

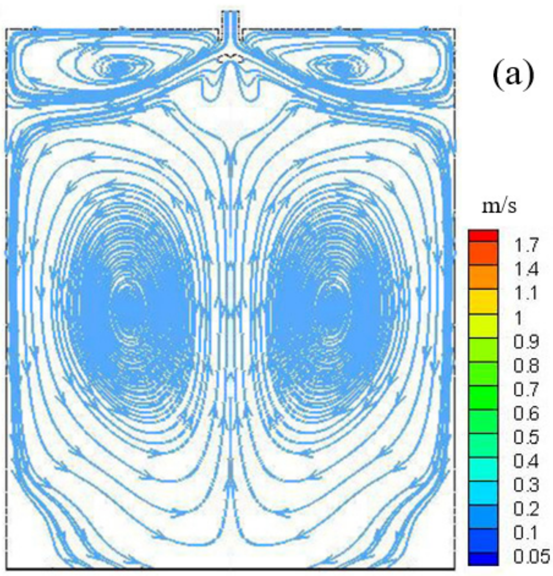

Figure 6. *Cont.*

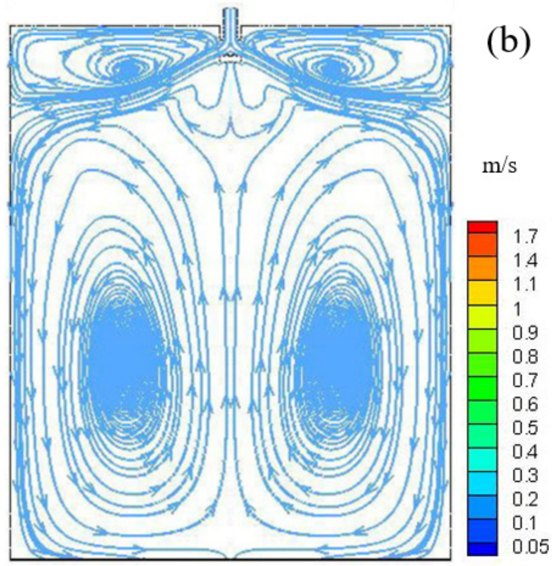

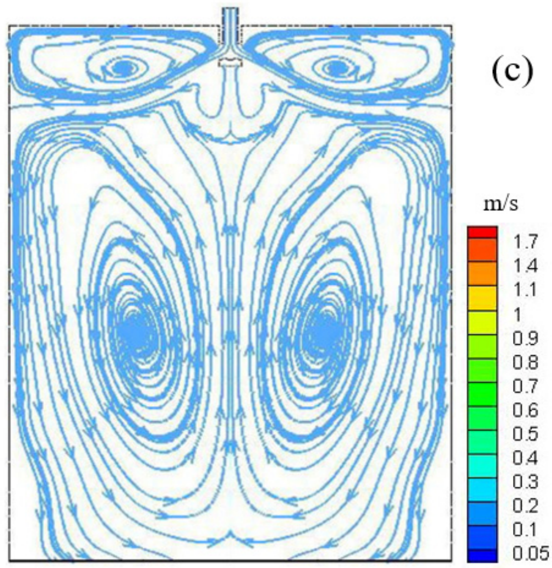

Figure 6. Trajectory line of molten steel: (**a**) 180 mm; (**b**) 200 mm; and (**c**) 220 mm.

Table 3. Whirlpool core positions and strike locations under different immersion depths.

Immersion Depth	Upper Whirlpool Centre	Lower Whirlpool Centre	Strike Position
180 mm	(0.626 m, −0.218 m)	(0.571 m, −1.557 m)	−0.438 m
200 mm	(0.612 m, −0.236 m)	(0.536 m, −1.718 m)	−0.476 m
220 mm	(0.590 m, −0.247 m)	(0.613 m, −1.860 m)	−0.499 m

The turbulent kinetic energies at the immersion depths of the three nozzles are compared in Figure 7. The turbulent kinetic energy of the free liquid surface change is inversely proportional to the immerse depth. The mold with a depth of 180 mm has a relatively large liquid surface velocity in the flow field, and the stability of the flow field is relatively poor. Additionally, the liquid surface velocity of the flow field is relatively more stable, and the average flow velocity is small, which is more conducive to maintaining the stability of the liquid surface. However, the fluctuation of the liquid surface is low, which is not conducive to slag, causing the upper part of the shell to solidify too quickly, and the lower part due to heat flow. Part of the shell melts, the temperature difference between the upper and lower sides becomes smaller, and the thickness of the mold shell is reduced, making it prone to breakout and bulging.

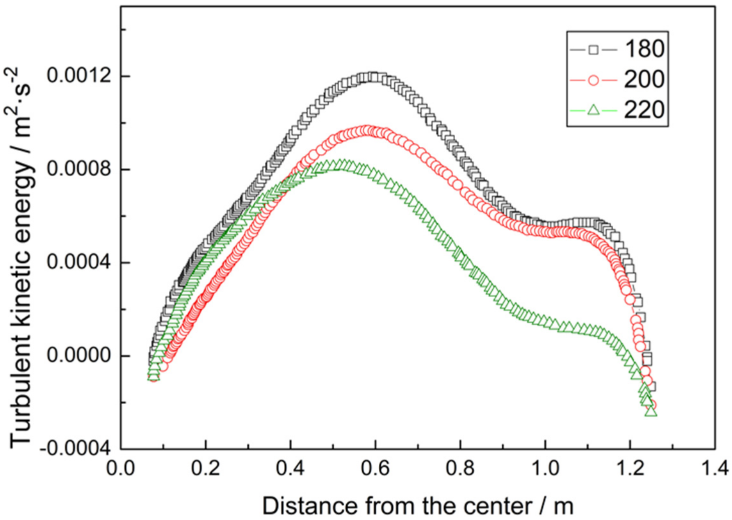

Figure 7. Turbulent kinetic energy at the free surface under different immersion depths.

Here, the principle of immersion depth selection is employed to consider the influence of the liquid level fluctuation and surface flow velocity on the melting and lubrication behavior of mold powder. In this example, the appropriate immersion depth is 200 mm.

3.3. Fluid Distribution under Different Slab Thicknesses

Figures 8–10 show the streamline diagram (a) and flow field distribution diagram (b) at different slab thicknesses of 220, 260, and 320 mm, respectively. Table 4 lists the changes in the location of the upper and lower return whirlpool centres and the strike locations of the narrow face. When the slab thickness is 220 mm, the location of the whirlpool centre in the upper reflow zone is (0.613, −0.199), and the position of the whirlpool centre in the lower reflow zone is (0.601, −1.727). When the slab thickness is 260 mm, the position of the whirlpool centre in the upper recirculation zone is (0.590, −0.247), which moves to the centre of the nozzle and the bottom of the mold; the position of the whirlpool centre in the lower recirculation zone is (0.613, −1.860), which moves downward. When the slab thickness is 320 mm, the location of the whirlpool centre in the upper reflow zone is (0.876, −0.241), which is closer to the narrow face than under the 220 mm thickness. Additionally, the surface flow velocity is higher, and the location of the whirlpool centre in the lower reflow zone is (0.660, −1.600), which is the closest to the free surface.

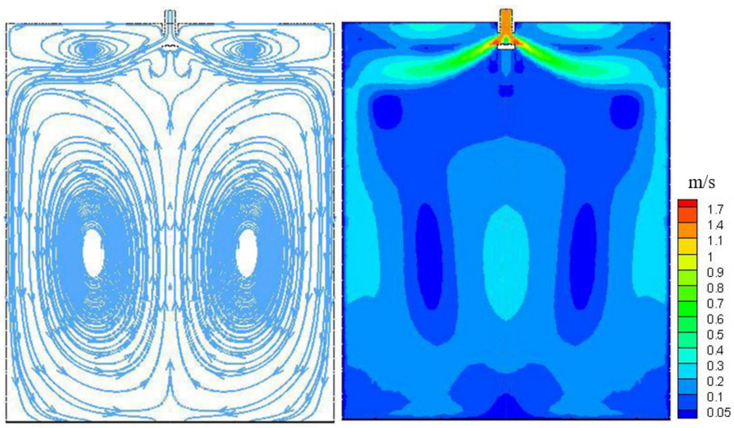

(a) (b)

Figure 8. Fluid contours: (**a**) trajectory line; and (**b**) flow field at a thickness of 220 mm.

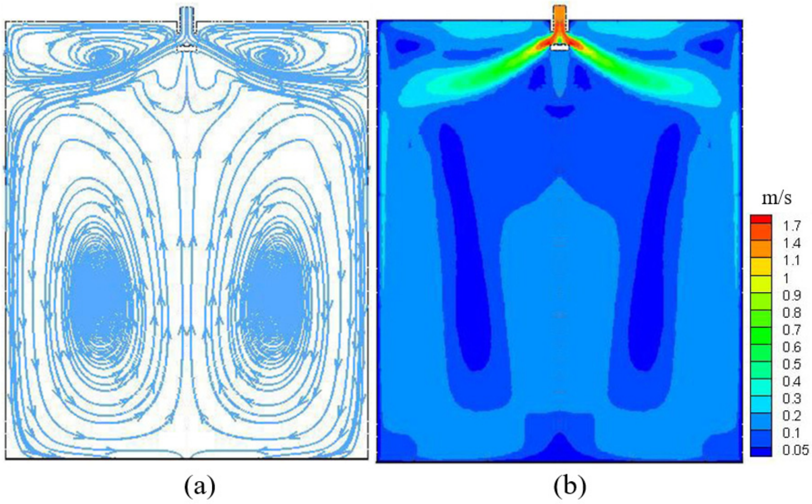

Figure 9. Fluid contours: (**a**) trajectory line; and (**b**) flow field at a thickness of 260 mm.

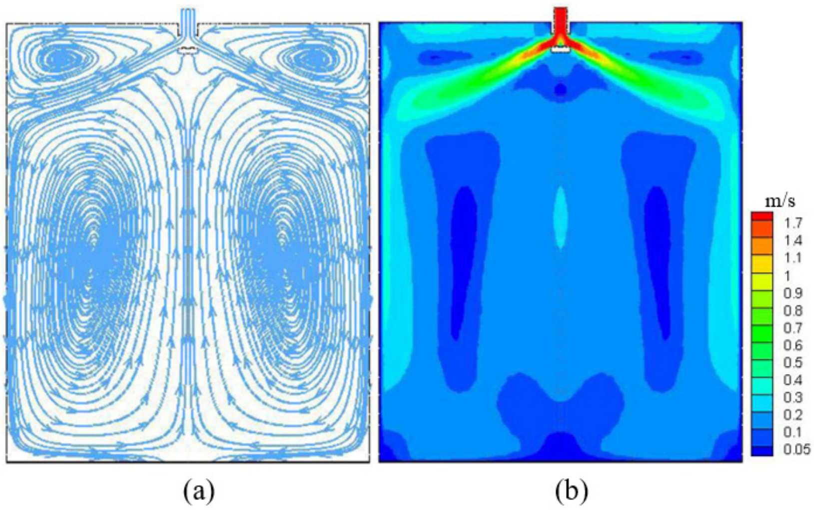

Figure 10. Fluid contours: (**a**) trajectory line; and (**b**) flow field at a thickness of 320 mm.

Table 4. Whirlpool core positions and strike locations under different slab thicknesses.

Slab Thickness	Upper Whirlpool Centre	Lower Whirlpool Centre	Strike Position
220 mm	(0.613 m, −0.199 m)	(0.601 m, −1.727 m)	−0.336 m
260 mm	(0.590 m, −0.247 m)	(0.613 m, −1.860 m)	−0.476 m
320 mm	(0.876 m, −0.241 m)	(0.660 m, −1.600 m)	−0.539 m

Figure 11 shows the change in turbulent kinetic energy. When the slab thickness increases, the strike locations of the narrow face are 0.336, 0.476, and 0.539 m, respectively, and the strike locations of the narrow face move downward. This may be due to the constant casting speed. When the thickness of the slab increases, the liquid molten steel passing through the cross-section of the slab increases per unit of time; that is, the increase in the amount of molten steel means that the molten steel enters the mold at a higher speed, and the main stream flows at a higher rate. The high momentum has an impact on the narrow face and moves the narrow face strike locations downward; however, due to the increase in the cross-sectional area of the slab, the molten steel requires more momentum to reach the meniscus position so that the upper reflux stream has a lower velocity and the turbulent kinetic energy of the liquid level is reduced. However, when the thickness increases to 320 mm, the section of the slab is too large, which causes the position of the upper recirculation whirlpool to move too far toward the narrow surface; therefore, the slab with a thickness of 320 mm has a lower turbulent kinetic energy at 0.3–0.6 m from the centre of the nozzle.

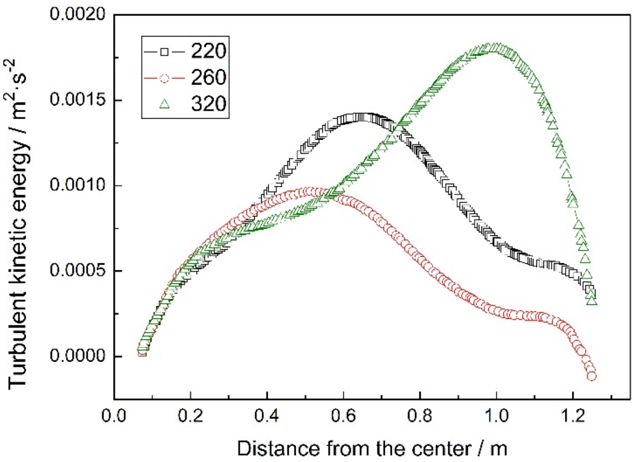

Figure 11. The influence of slab thickness on the turbulent kinetic energy.

3.4. Fluid Distribution under Different Slab Widths

Figures 12–14 show the streamline diagram (a) and flow field distribution diagram (b) of the mold when the slab widths are 2300, 2500, and 2700 mm, respectively. Table 5 lists the changes in the location of the upper and lower return whirlpool centres and the strike locations of the narrow face. When the slab width is 2300 mm, the position of the whirlpool centre in the upper reflow zone is (0.542, −0.222), and the position of the whirlpool centre in the lower reflow zone is (0.534, −1.851). When the slab width is 2500 mm, the position of the whirlpool centre in the upper recirculation zone is (0.590, −0.247), and the position of the whirlpool centre in the lower recirculation zone is (0.613, −1.860), which shows little change compared with the width of 2300 mm. When the slab width is 2700 mm, the position of the whirlpool centre in the upper recirculation zone is (0.655, −0.222), which moves to the narrow surface of the slab with a larger range and has a higher surface velocity. The position of the whirlpool centre in the lower recirculation zone is (0.652, −1.650), which is the closest to the free liquid surface. The strike locations of the narrow surface are 0.354, 0.476, and 0.460 m, respectively, and the strike locations increase first and then decrease.

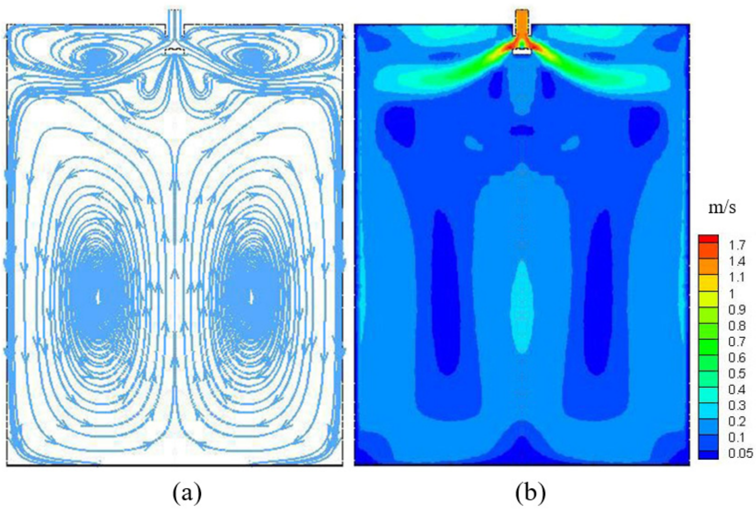

Figure 12. Fluid contours: (**a**) trajectory line; and (**b**) flow field at a 2300 mm width.

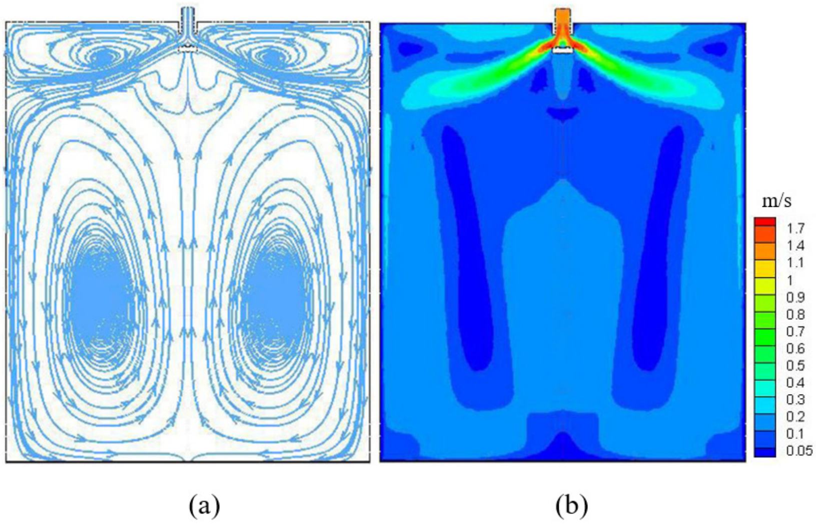

Figure 13. Fluid contours: (**a**) trajectory line; and (**b**) flow field at a 2500 mm width.

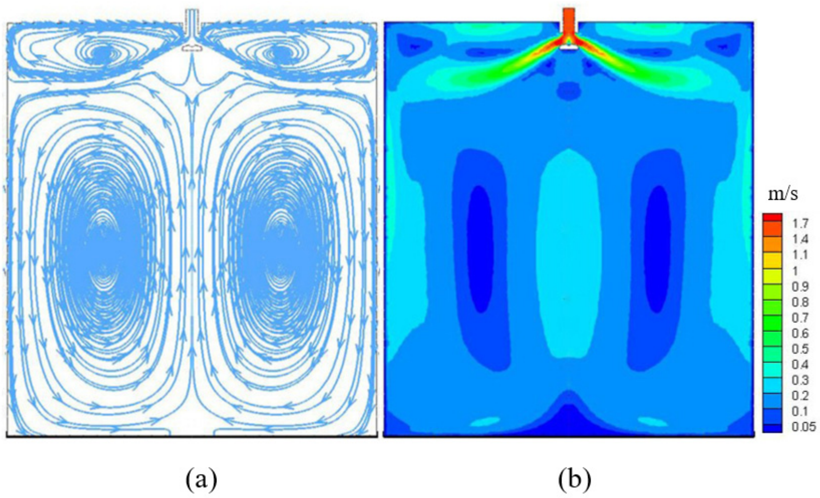

Figure 14. Fluid contours: (**a**) trajectory line; and (**b**) flow field at a 2700 mm width.

Table 5. Whirlpool core positions and strike locations under different slab widths.

Slab Width	Upper Whirlpool Centre	Lower Whirlpool Centre	Strike Position
2300 mm	(0.542 m, −0.222 m)	(0.534 m, −1.851 m)	−0.354 m
2500 mm	(0.590 m, −0.247 m)	(0.613 m, −1.860 m)	−0.476 m
2700 mm	(0.655 m, −0.222 m)	(0.652 m, −1.650 m)	−0.460 m

Figure 15 shows the change of free liquid surface turbulent kinetic energy under different slab widths. When the slab width increases from 2300 to 2500 mm, the free surface turbulent kinetic energy decreases. However, when it increases to 2700 mm, the maximum free surface turbulent kinetic energy increases to 0.00245 $m^2 \cdot s^{-2}$. This may be due to the section of the slab being too large, whereby the liquid molten steel with the same initial velocity moves from the nozzle to the narrow surface of the mold and flows over a larger distance, which increases the momentum loss. The position of the main stream impacting the narrow surface moves relatively upward, and the positions of the upper and lower whirlpool centres move toward the narrow surface and upward. Additionally, the velocity of the fluid when it reaches the meniscus becomes faster as a whole, making the turbulent kinetic energy at the free liquid surface larger. This phenomenon does not occur when the slab section is within a reasonable range. When the slab width changes, the change trend of the flow field in the mold is consistent with the thickness change; thus, in actual production, various factors should be comprehensively considered to formulate a reasonable slab thickness and width scheme.

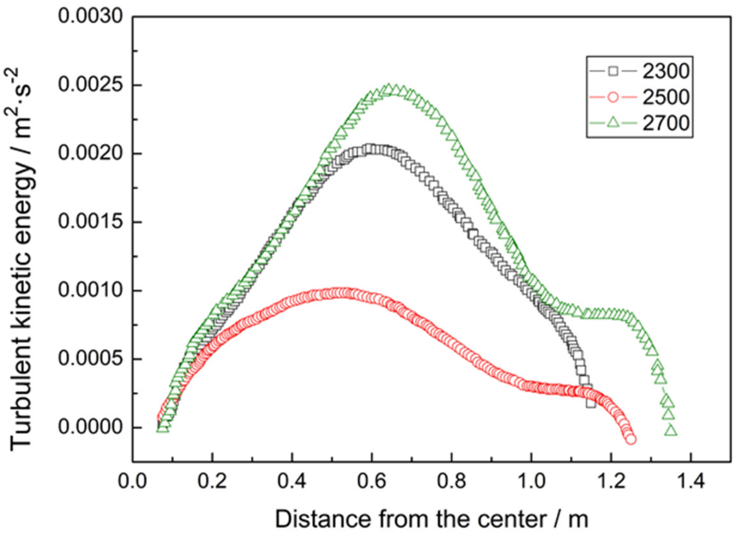

Figure 15. Influence of slab width on the turbulent kinetic energy at the free surface.

4. Conclusions

(1) When the casting speeds increased from 0.6 to 1.0 m/min, the strike positions of the narrow surface were 0.439, 0.476, and 0.480 m away from the meniscus, respectively. The molten steel flow speed in the mold becomes significantly faster, the momentum of the liquid molten steel increases and the velocity distribution of the upper and lower reflux zones change significantly;

(2) When the immersion depths increased from 180 to 220 mm, the impact depth of the stream at the exit of the nozzle side hole moved downward, the lower recirculation zone moved to the centre and bottom of the slab, and the upper recirculation zone moved downward;

(3) When the slab thickness increased from 220 to 320 mm, the strike locations of the narrow face moved downward; so, the quality of the thick slab is not easy to control;

(4) When the slab width increased from 2300 to 2700 mm, the strike locations of the narrow surface were 0.354, 0.476, and 0.460 m, respectively, and the strike locations of the narrow surface increased first and then decreased. When the slab width increases from 2300 to 2500 mm, the free surface turbulent kinetic energy decreases; however, when it increases to 2700 mm, the maximum free surface turbulent kinetic energy increases to 0.00245 $m^2{\cdot}s^{-2}$. So, the quality of the wider slab is more difficult to control than the quality of the narrower slab.

Author Contributions: Data curation, J.Z., Y.Z. and T.L.; methodology, G.Z.; and writing—original draft, F.D. All authors have read and agreed to the published version of the manuscript.

Funding: This research received no external funding.

Institutional Review Board Statement: Not applicable.

Informed Consent Statement: Not applicable.

Data Availability Statement: Not applicable.

Conflicts of Interest: The authors declare no conflict of interest.

References

1. Khan, Z.; Rasheed, H.U.; Khan, I.; Abu-Zinadah, H.; Aldahlan, M.A. Mathematical simulation of casson MHD flow through a permeable moving wedge with nonlinear chemical reaction and nonlinear thermal radiation. *Materials* **2022**, *15*, 747. [CrossRef]
2. Zeeshan. Second law and entropy generation analysis of magnetized viscous fluid flow over a permeable expandable sheet with nonlinear thermal radiation: Brownian and thermophoresis effect. *Adv. Mech. Eng.* **2022**, *14*, 16878140221075295. [CrossRef]
3. Thomas, B.G. Modeling of the continuous casting of steel—Past, present, and future. *Metall. Mater. Trans. B* **2002**, *33*, 795–812. [CrossRef]
4. Du, F.M.; Chen, C.D.; Zhang, K.G. Fluid characteristics analysis of the lubricating oil film and the wear experiment investigation of the sliding bearing. *Coatings* **2022**, *12*, 67. [CrossRef]
5. Takatani, K.; Tanizawa, Y.; Mizukami, H.; Nishimura, K. Mathematical model for transient fluid flow in a continuous casting mold. *ISIJ Int.* **2001**, *41*, 1252–1261. [CrossRef]
6. Zhang, W.; Gao, J.; Rohatgi, P.K.; Zhao, H.; Li, Y. Effect of the depth of the submerged entry nozzle in the mold on heat, flow and solution transport in double-stream-pouring continuous casting. *J. Mater. Process. Technol.* **2009**, *209*, 5536–5544. [CrossRef]
7. Torren, A.E.; Morales, R.D.; Garcia-Hernandez, S.; Najera-Bastida, A.; Sandoval-Ramos, A. Influence of straight nozzles on fluid flow in mold and billet quality. *Metall. Mater. Trans. B* **2008**, *39*, 840–852. [CrossRef]
8. Wang, C.N.; Wen, L.Y.; Chen, D.F.; Zhang, D.J.; Jin, X. Effect of bottom structure of submerged entry nozzle on flow field and temperature field in continuous casting mold. *Iron Steel* **2010**, *45*, 37–42. [CrossRef]
9. Deng, X.X.; Wang, Q.Q.; Qian, L.; Wang, X.H.; Huang, F.X. Water model optimization of three-port submerged entry nozzle feeding a funnel-shaped thin slab mold. *Iron Steel* **2012**, *47*, 26–32. [CrossRef]
10. Quan, Y.; Thomas, B.G.; Vanka, S.P. Study of transient flow and particle transport in continuous steel caster molds: Part I Fluid flow. *Metall. Mater. Trans. B* **2004**, *35*, 685–702. [CrossRef]
11. Ho, Y.H.; Chen, C.H.; SWang, W.S. Analysis of molten steel flow in slab continuous caster mold. *ISIJ Int.* **1994**, *3*, 255–264. [CrossRef]
12. Yang, H.L.; Zhang, X.Z.; Deng, K.; Li, W.; Zhao, L. Mathematical simulation on coupled flow, heat, and solute transport in slab continuous casting process. *Metall. Mater. Trans. B* **1998**, *29*, 1345–1356. [CrossRef]
13. Thomas, B.G.; Zhang, L. Mathematical modeling of fluid flow in continuous casting. *ISIJ Int.* **2001**, *10*, 1181–1193. [CrossRef]
14. Wang, Y.F.; Zhang, L.F. Transient fluid flow phenomena during continuous casting: Part ii-cast speed change, temperature fluctuation, and steel grade mixing. *ISIJ Int.* **2010**, *50*, 1783–1791. [CrossRef]
15. Tian, C.; Yuan, L.; Yao, X.L.; Liu, Z.L.; Song, Y.; Liu, G.Q.; Yu, J.K.; Li, H.X. Measurement model of molten steel flow velocity in the continuous casting mould based on the Seebeck principle. *Ironmak. Steelmak.* **2021**, *49*, 24–28. [CrossRef]
16. Domitner, J.; Wu, M.H.; Ludwig, A. Numerical study about the influence of small casting speed variations on the metallurgical length in continuous casting of steel slabs. *Steel Res. Int.* **2015**, *86*, 184–188. [CrossRef]
17. Tripathi, A.; Ajmani, S.K.; Chandra, S. Numerical investigation of bias flow in a slab caster mould. *Can. Metall. Quart.* **2021**, *60*, 203–214. [CrossRef]
18. Bai, H.; Thomas, B.G. Turbulent flow of liquid steel and argon bubbles in slide-gate tundish nozzles: Part II. Effect of opera-tion conditions and nozzle design. *Metall. Mater. Trans. B* **2001**, *32*, 269–284. [CrossRef]
19. Gupta, D.; Chakraborty, S.; Lahiri, A.K. Asymmetry and oscillation of the fluid flow pattern in a continuous casting mould: A water model study. *ISIJ Int.* **1997**, *37*, 654–658. [CrossRef]
20. Takatani, K. Effects of electromagnetic brake and meniscus electromagnetic stirrer on transient molten steel flow at meniscus in a continuous casting mold. *ISIJ Int.* **2003**, *6*, 915–922. [CrossRef]
21. Li, B.K.; Tsukihashi, F. Effects of electromagnetic brake on whirlpool flows in thin slab continuous casting mold. *ISIJ Int.* **2006**, *12*, 1833–1838. [CrossRef]
22. Shamsi, M.R.R.I.; Ajmani, S.K. Three dimensional turbulent fluid flow and heat transfer mathematical model for the analysis of a continuous slab caster. *ISIJ Int.* **2007**, *3*, 433–442. [CrossRef]
23. Lu, B.W.; Yuan, F.L.; Wang, H.L.; Bai, H. Water model experimental study on the behavior of fluid flow in slab caster mold. *Res. Iron Steel* **2015**, *43*, 24–27. [CrossRef]